CHEMISTRY
A EUROPEAN JOURNAL

DOI: 10.1002/chem.200800426

Definition of Magneto-Structural Correlations for the Mn^{II} Ion

Carole Duboc,*[a, b] Marie-Noëlle Collomb,[a] Jacques Pécaut,[c] Alain Deronzier,[a] and Frank Neese*[d]

Abstract: The electronic properties of the high spin mononuclear Mn^{II} complexes $[Mn(tpa)(NCS)_2]$ (**1**) (tpa = tris-2-picolylamine), $[Mn(t\mathrm{Bu}_3\text{-terpy})_2](PF_6)_2$ (**2**) ($t\mathrm{Bu}_3$-terpy = 4,4′,4″-tri-*tert*-butyl-2,2′:6′,2″-terpyridine) and $[Mn(terpy)_2](I)_2$ (**3**) (terpy = 2,2′:6′,2″-terpyridine) with an N6 coordination sphere have been determined by multi-frequency EPR spectroscopy. The X-ray structures of **1**·CH_3CN and **2**·$C_4H_{10}O$·0.5 C_2H_5OH·0.5 CH_3OH reveal that the Mn^{II} ion lies at the center of a distorted octahedron. The *D*-values of **1**–**3** all fall in the narrow range of 0.041 to 0.105 cm^{-1}. The comparison of the results reported here and those found in the literature is consistent with the following observation: the *D* value is sensitive to the coordination number (6 or 5) of the Mn^{II} ion as long as the coordination sphere involves only nitrogen and/or oxygen based ligands. This magneto-structural correlation has been analyzed in this work though DFT model calculations. The zero-field splitting (zfs) parameters of **1**–**3** have been calculated and are in reasonable agreement with the experimental values. Hypothetical simplified models $[Mn(NH_3)_x(OH_2)_y]^{2+}$ ($x+y=5$ or 6 and $[Mn(NH_3)_5X]^+$ (X = OH, Cl)) have been constructed to investigate the origin of the zfs. This investigation reveals i) that *D* is sensitive to the coordination number (5 or 6) of the Mn^{II} ion, ii) for the five coordinate systems the major contribution to *D* is the spin-orbit coupling part, iii) for the six coordinate systems the major contribution to *D* is the spin–spin interaction and iv) the deprotonation of a water ligand leads to an increase of *D*, consistent with the relative ligand fields of OH^- versus H_2O.

Keywords: density functional calculations · magnetic properties · manganese · metalloenzymes · zero-field splitting

Introduction

The correlation of spectroscopic and structural properties of transition metal complexes is of crucial importance. Such correlations allow predictions as to the structure of complexes for which no such data are available, as can be the case in biological systems.

Here, we focus on Mn^{II} complexes that are widely present in numerous enzymes, as an essential ingredient of their active site. The metallic ion is implicated in redox reactions or in non-redox processes (catalysis or structural role).[1] In addition, the paramagnetic Mn^{II} ion is commonly used as a probe replacing the Zn^{II}, Mg^{II}, or Ca^{II} ions in other biological systems.[2]

The $3d^5$ Mn^{II} ion is generally high-spin ($S=5/2$, $I=5/2$) and its electronic properties can usually be well described by the following spin Hamiltonian in Equation (1):

$$H = \beta BgS + IAS + D[S_z^2 - 1/3 S(S+1)] + E(S_x^2 - S_y^2) \qquad (1)$$

The two first terms represent the Zeeman and electron nu-

[a] Dr. C. Duboc, Dr. M.-N. Collomb, Dr. A. Deronzier
Département de Chimie Moléculaire
UMR 5250, ICMG FR 2607, CNRS, Université Joseph Fourier
BP 53, 38041 Grenoble Cedex 9 (France)
Fax: (+33)476514267
E-mail: carole.duboc@ujf-grenoble.fr

[b] Dr. C. Duboc
Grenoble High Magnetic Field Laboratory
UPR 5021, CNRS, BP 166, 38042 Grenoble Cedex 9 (France)

[c] J. Pécaut
DRFMC-Service de Chimie Inorganique et Biologique
Laboratoire Coordination et Chiralité, CEA-Grenoble
38054 Grenoble cedex 9 (France)

[d] Prof. Dr. F. Neese
Institut für Physikalische und Theoretische Chemie
University of Bonn, Wegelerstrasse 12, 53115 Bonn (Germany)
Fax: (+49)0228-73-9064
E-mail: neese@thch.uni-bonn.de

Supporting information for this article is available on the WWW under http://www.chemeurj.org/ or from the author.

clear hyperfine interactions, respectively, whereas the last two define the second-order (bilinear) zfs interaction with D and E representing the axial and rhombic parts, respectively. For $S = {}^5/_2$ quartic terms in the effective spin can arise.[3]

The most powerful technique for accurately determining the spin-Hamiltonian parameters (SHPs) of biological[4] or synthetic[5] Mn^{II} complexes is EPR spectroscopy and more particularly high field/high frequency EPR (HF-EPR). HF-EPR has been successfully used in many applications that probe the structure around the ion, the molecular mechanism in which the ion is implicated, or the incorporation of the metal in a biological host. Nevertheless, the lack of magneto-structural correlations generally restricts the analysis.[4e]

In this context, the definition of such correlations represents a crucial point in order to link a specific molecular geometry to the observed SHPs, in particular *D*. Indeed, this term, ranging from values close to zero up to 1.5 cm^{-1},[6] is the most sensitive parameter in the spin Hamiltonian with respect to geometric variations. However, progress in this field requires combined experimental and theoretical methods to determine the nature of the zfs. We have already successfully used this approach in the investigation of mononuclear halide Mn^{II} complexes.[7] The correlation between the magnitude of D and the nature of the halide has been experimentally determined by HF-EPR and has been supported and understood with the help of density functional theory (DFT) calculations.

Here, our goal is to extend this previous work[7,8] to mononuclear Mn^{II} complexes with only oxygen- or nitrogen-based ligands, a coordination sphere typically found in metalloenzymes. The main aim of this work is to define magneto-structural correlations that may prove to be useful to the biochemical community. In particular, we focus this study on five and six coordinate systems, which are the most commonly found in metalloenzymes. Based on experimental observations, it was generally proposed for such Mn^{II} complexes that the magnitude of D is governed by the coordination number of the Mn^{II} ion with higher values observed for five coordinate compounds compared those that were six coordinate.[4a,c]

However there is a need for experimental data on mononuclear Mn^{II} complexes with an N6 coordination sphere for which both X-ray structure and zfs have been measured. Consequently, in this paper, we determine, through the help of X-band as well as HF-EPR techniques, the SHPs of three N6 Mn^{II} compounds: $[Mn(tpa)(NCS)_2]$ (**1**) (tpa = tris-2-picolylamine), $[Mn(t\mathrm{Bu}_3\text{-terpy})_2](PF_6)_2$ (**2**) ($t\mathrm{Bu}_3$-terpy = 4,4′,4″-tri-tert-butyl-2, 2′:6′,2″-terpyridine) and $[Mn(terpy)_2](I)_2$ (**3**) (terpy = 2,2′:6′,2″-terpyridine). The X-ray structure of **1** and **2** is also determined, whereas the structure of **3** has already been reported.[9] Based on these X-ray structures, we investigated the zfs of **1**–**3** by DFT techniques. The results have been compared with our previous studies performed on complexes with a N5 coordination sphere.[5d–e,8] Furthermore, to understand the discrepancy observed for D between the five and six coordinate complexes, we developed hypothetical theoretical models that allowed us to identify and quantify the different contributions to D for both types of coordination.

Results and Analysis

Synthesis and crystal structure determination of complexes 1 and 2: The crystal structures of **1**·CH_3CN and **2**·$C_4H_{10}O$·0.5 C_2H_5OH·0.5 CH_3OH have been solved by single crystal X-ray crystallography. Table 1 provides the principal crystallographic data and Table 2 and Table 3 selected bond distances and angles, for **1** and **2**, respectively. Figure 1 displays ORTEP views of the two complexes. Complex **1** has been isolated by a synthetic way different from that used by Oshio et al.[10]

In both complexes, the Mn^{II} ion is pseudooctahedrally coordinated by six nitrogen atoms from: one tpa and two *cis*

Table 1. Principal crystallographic data and parameters for the $[Mn(tpa)(NCS)_2]$ $CH_3CN·H_2O$ (**1**·CH_3CN) and $[Mn(t\mathrm{Bu}_3\text{-terpy})_2](PF_6)_2$·$C_4H_{10}O$·0.5 C_2H_5OH·0.5 CH_3OH (**2**·$C_4H_{10}O$ ·0.5 C_2H_5OH·0.5 CH_3OH) complexes.

Compound	**1**·CH_3CN	**2**·$C_4H_{10}O$·0.5 C_2H_5OH ·0.5 CH_3OH
chemical formula	$C_{22}H_{21}S_2MnN_7$	$C_{59.5}H_{85}F_{12}MnN_6O_2P_2$
formula weight	502.52	1261.61
crystal system	orthorhombic	monoclinic
space group	P2(1)2(1)2(1)	P2(1)/c
a [Å]	11.835(2)	14.013(6)
b [Å]	13.302(3)	20.628(8)
c [Å]	15.750(3)	24.989(10)
α [°]	90	90
β [°]	90	103.197(7)
γ [°]	90	90
volume [$Å^3$]	2479.4(9)	7033(5)
T [K]	298(2)	293(2)
λ [Å]	0.71073	0.71073
θ [$mg\,m^{-3}$]	1.346	1.191
Z	4	4
μ [mm^{-1}]	0.724	0.306
$F(000)$	1036	2652
reflections collected	7161	25495
$R1$[a]	0.0289	0.0657
$wR2$[b]	0.0669	0.2117

[a] $R1 = \Sigma\,||F_o| - |F_c||/\Sigma\,|F_o|$. [b] $wR2 = [(\Sigma w(|F_o| - |F_c|)^2/\Sigma wF_o^2)]^{1/2}$

Table 2. Selected bond distances [Å] and angles [°] for **1**·CH_3CN.

Mn–N(21)	2.113(2)	Mn–N(22)	2.167(2)
Mn–N(1)	2.3290(19)	Mn–N(2)	2.2722(17)
Mn–N(3)	2.3567(17)	Mn–N(4)	2.2646(19)
N(1)–Mn–N(2)	74.71(6)	N(2)–Mn–N(21)	107.12(8)
N(1)–Mn–N(3)	74.56(7)	N(2)–Mn–N(22)	90.31(7)
N(1)–Mn–N(4)	73.38(7)	N(3)–Mn–N(21)	90.16(8)
N(2)–Mn–N(3)	75.84(6)	N(3)–Mn–N(22)	164.52(7)
N(3)–Mn–N(4)	98.09(7)	N(4)–Mn–N(21)	104.28(8)
N(2)–Mn–N(4)	147.98(7)	N(4)–Mn–N(22)	89.98(7)
N(1)–Mn–N(21)	163.83(8)	N(21)–Mn–N(22)	100.69(9)
N(1)–Mn–N(22)	95.34(8)		

Table 3. Selected bond distances [Å] and angles [°] for **2**·$C_4H_{10}O$·0.5 C_2H_5OH·0.5 CH_3OH.

Mn–N(1)	2.222(4)	Mn–N(31)	2.227(4)
Mn–N(2)	2.183(4)	Mn–N(32)	2.198(4)
Mn–N(3)	2.258(4)	Mn–N(33)	2.236(4)
N(2)–Mn–N(32)	163.94(13)	N(1)–Mn–N(33)	93.57(14)
N(2)–Mn–N(1)	73.12(13)	N(31)–Mn–N(33)	143.94(14)
N(32)–Mn–N(1)	121.15(13)	N(2)–Mn–N(3)	72.05(13)
N(2)–Mn–N(31)	114.67(14)	N(32)–Mn–N(3)	94.32(13)
N(32)–Mn–N(31)	72.75(13)	N(1)–Mn–N(3)	144.48(14)
N(1)–Mn–N(31)	98.17(14)	N(31)–Mn–N(3)	90.05(14)
N(2)–Mn–N(33)	101.36(14)	N(33)–Mn–N(3)	99.85(15)
N(32)–Mn–N(33)	71.99(13)		

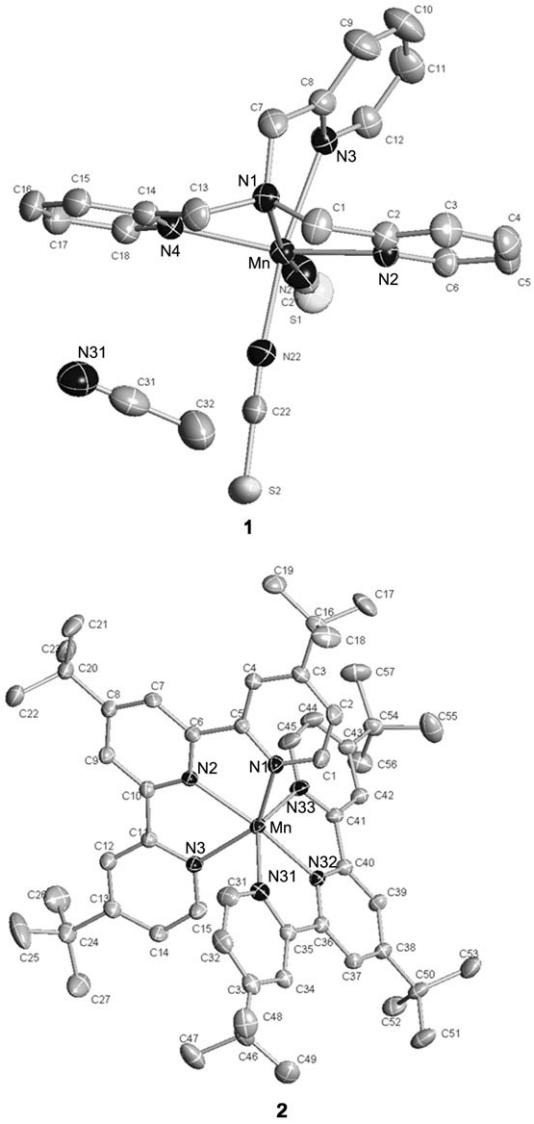

Figure 1. ORTEP diagrams showing the molecular structures of complexes **1** and **2**. The hydrogen atoms have been omitted for clarity.

NCS ligands in **1**, and two meridional *t*Bu_3-terpy ligands in **2**. The coordination geometry around the Mn^{II} is highly distorted from octahedral, owing to the spatially constrained nature of the *t*Bu_3-terpy and tpa ligands. The structure of **1**·CH_3CN is very similar to that previously determined.[10] The coordination mode of the NCS ligands imposed by the nature of the tpa ligand is *cis*. As previously observed in [Mn(tpa)X_2] (X = I, Br, Cl),[7] the Mn–N_{tpa} (Mn–N(1) and Mn–N(3)) bonds *trans* to the NCS are consistently longer than the other Mn–N_{tpa} bonds (Mn–N(2) and Mn–N(4)). The Mn–N_{NCS} bond lengths are located in the range of values found in other Mn^{II}-N_{NCS} complexes (Mn–N_{NCS}: 2.062–2.185 Å).[5d] The structure of **2** is comparable with that of **3**.[9] The Mn–N in **2** bond lengths are, nevertheless, slightly shorter by ≈0.01 Å than those in **3** in accordance with the electron-donating character of the tertiobutyl substituents. In addition, as always observed in terpyridine Mn complexes,[5d–f,9,11] the Mn–$N_{central}$ bond length is smaller than that of the Mn–N_{distal} bonds. This distortion induces a tetragonal compression of the octahedral coordination sphere along the $N_{central}$–Mn–$N_{central}$ axis in the bis-terpyridine complexes **2** and **3**.

Multifrequency EPR on complexes 1–3: A powder multifrequency EPR study has been performed on compounds **1–3** to precisely determine their SHPs and in particularly the zero-field splitting-interaction. HF-EPR spectra of **1** ($\tilde{\nu}$ = 95 and 190 GHz) are reported in Figure 2. At both frequencies the high field limit conditions are reached (comparable total width of the spectra 0.69 and 0.67 mT at $\tilde{\nu}$ = 95 and 190 GHz, respectively). Therefore D can be estimated from the field difference between the furthest transition from the center of the spectra, $|^5/_2;-^5/_2> \rightarrow |^5/_2;-^3/_2>$ transition along z, (3.02 and 6.42 T) and g = 2.00 (3.42 and 6.80 T), which is equal to $4D$ (under the plausible approximation that $g_{x,y,z} = g_e = 2.00$): 0.09 cm^{-1}. The low field position of the $|^5/_2;-^5/_2> \rightarrow |^5/_2;-^3/_2>z$ transition compared to g = 2 also allows the determination of the negative sign of D. At $\tilde{\nu}$ = 95 GHz, a "forbidden" transition is observed at low field with a relatively weak intensity (Figure 2, top, inset) while it is absent at 190 GHz, in agreement with a small D value. The accurate determination of the SHPs from simulations of the experimental HF-EPR spectra using a full-matrix diagonalization procedure of the spin Hamiltonian in Equation (1) corroborates this reasoning (Table 4). For the neat powder samples, the hyperfine interaction was not resolved and consequently not taking into account for the simulations.

Complex **3** has been investigated as a neat powder and also magnetically diluted into a Zn(II) host named [Zn(Mn)(tolyl-terpy)$_2$](PF_6)$_2$. The effect of the temperature on the shape of the HF-EPR spectra recorded at $\tilde{\nu}$ = 285 GHz on the neat powder is shown in Figure 3. The negative sign of D is unambiguously determined at T = 5 K and the simulations of both spectra afford the SHP (Table 4). The features are less resolved than in complex **1** since D is noticeably smaller with a same line-width.

If **3** is doped into a Zn(II) host, the shape of the spectrum changes drastically. Features are present in a smallest field range (≈60 mT) corresponding to the central

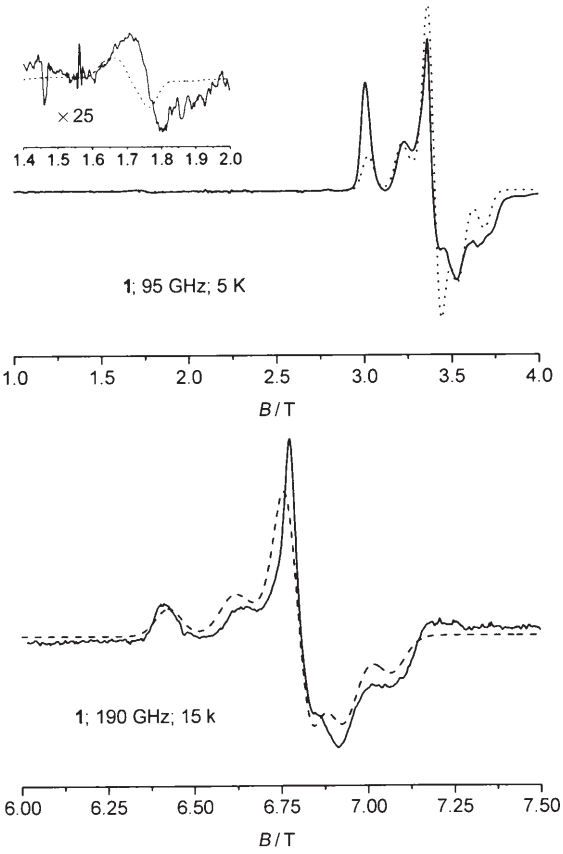

Figure 2. Experimental (——) and simulated (-----) neat powder HF-EPR spectra of complex **1** recorded at $\tilde{\nu}=95$ GHz and $T=5$ K (top) and $\tilde{\nu}=190$ GHz and $T=15$ K (bottom). Parameters used for the simulation: $D=-0.085(4)$ cm^{-1}, $E=-0.015(2)$ cm^{-1}, $g_x=g_y=g_z=2.000(1)$, $W=0.35$ mT.

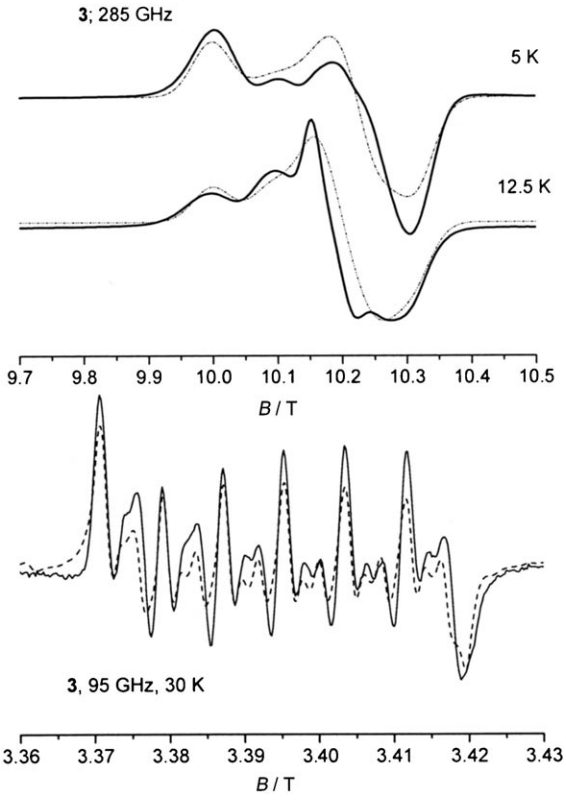

Figure 3. Experimental (——) and simulated (-----) HF-EPR spectra of complex **3** recorded at $\tilde{\nu}=285$ GHz on the neat powder (top) and at $\tilde{\nu}=95$ GHz and on the $[Zn(Mn)(terpy)_2]^{2+}$ (bottom). Parameters used for the simulation: $D=-0.042(3)$ cm^{-1}, $E=-0.005(1)$ cm^{-1}, $g_x=g_y=g_z=2.000(1)$, $W=0.35$ mT (top), $D=-0.058(1)$ cm^{-1}, $E=-0.006(1)$ cm^{-1}, $g_x=g_y=g_z=2.000(1)$, $A_x=A_y=A_z=76(1)$ G, $W=10$ G (bottom).

$|^5/_2;-^1/_2> \rightarrow |^5/_2;+^1/_2>$ transition. The complexity of the spectra originates not only from the hyperfine interaction, but also from the second-order contributions of the zfs, which lead to the detection of more than the expected six transitions.[2b,4c–e,8e,12] The simulation of the HF-spectra recorded at different frequencies reveals a significant discrepancy between both D values (-0.042 and -0.058 cm^{-1} as a neat powder and magnetically diluted, respectively). During the preparation of this manuscript, HF-EPR spectra (powder and in solution) of **3** have been published.[5g] The D-value has been extracted only from spectra recorded in solution and found to be equal to -0.051 cm^{-1}. From these three experimental D values determined on the same complex, but in different environments, it appears that small structural changes can lead to noticeable variations in the D value.

Table 4. Experimental and calculated zero-field splitting parameters and D contributions of complexes **1**–**3**, $[Mn(terpy)(NCS)_2]$ and $[Mn(t\mathrm{Bu}_3\text{-terpy})(N_3)_2]$.

	1	**2**	**3**	$[Mn(terpy)(NCS)_2]$[a]	$[Mn(t\mathrm{Bu}_3\text{-terpy})(N_3)_2]$[b]
Experimental					
D [cm^{-1}]	−0.085	−0.073	−0.042	−0.300	−0.250
E [cm^{-1}]	−0.015	−0.015	−0.005	−0.050	−0.044
$\lvert E/D \rvert$	0.176	0.205	0.119	0.020	0.176
Calculated					
D [cm^{-1}]	−0.075	+0.111	+0.068	−0.504	−0.347
D_{SOC} [cm^{-1}][c]	−0.031	+0.049	−0.006	−0.317	−0.247
$\alpha\rightarrow\alpha$[d]	−0.034	+0.027	+0.032	−0.140	−0.146
$\beta\rightarrow\beta$[d]	−0.027	+0.001	+0.009	−0.032	−0.021
$\alpha\rightarrow\beta$[d]	0.007	+0.018	−0.039	−0.144	−0.073
$\beta\rightarrow\alpha$[d]	0.023	+0.003	−0.007	−0.001	−0.007
D_{SS} [cm^{-1}][e]	−0.044	+0.062	+0.073	−0.187	−0.099
1-center[f]	−0.049	+0.059	+0.067	−0.181	−0.091
2-center [f]	+0.005	+0.002	+0.006	−0.006	−0.008
E [cm^{-1}]	−0.009	+0.021	+0.002	−0.034	−0.046
$\lvert E/D \rvert$	0.123	0.183	0.036	0.067	0.130

[a] Ref. [5d,8]; [b] Ref. [5e,8]; [c] the SOC contribution to the total D value; [d] the excitations contributing to the total D_{SOC} value, [e] the SS contribution to the total D value; [f] the n-center contributions to the total D_{SS} value.

For complex **2**, a X-band EPR spectrum is displayed in Figure 4. The SHPs have been determined (Table 4) by simulating HF-EPR spectra (data not shown). At low

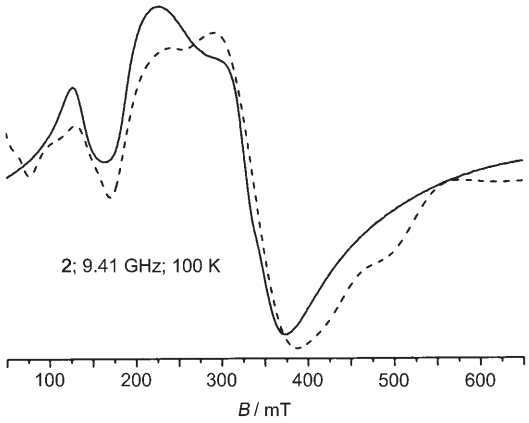

Figure 4. Experimental (——) and simulated (-----) X-band EPR spectrum of complex **2** recorded on the neat powder. Parameters used for the simulation: $D=-0.073(2)$ cm^{-1}, $E=-0.015(1)$ cm^{-1}, $g_x=g_y=g_z=2.000(1)$ and $W_x=W_y=0.40$, $W_z=0.35$ mT.

frequency, even though D (0.073 cm^{-1}) is relatively small compared to the energy provided by the X-band spectrometer (0.3 cm^{-1}), a unique set of SHPs and the sign of D can not be determined with confidence.

Density functional calculations

*Calculations on complexes **1–3***: In previous works,[7,8] we have shown that our DFT approach is suitable for mononuclear Mn^{II} complexes, which contain halide ligands (five and six coordinate) or are five coordinate without a halide ligand. Here, we perform DFT calculations on complexes **1–3** to investigate the reliability of the DFT method for Mn^{II} complexes with a N6 coordination sphere.

The calculations have been directly carried out on the crystal structures of complexes **1–3** without optimization of the geometries. We have previously observed that the use of theoretically optimized geometries leads to a significant deterioration of the theoretical predictions relative to the experimental geometries derived from X-ray diffraction.[8] Furthermore, as experimentally observed for **3**, D is sensitive to small structural changes (see above). The experimental and calculated zfs parameters of **1–3** are given in Table 4 together with previously reported values determined for the mononuclear Mn^{II} complexes with a N5 coordination sphere, $[Mn(terpy)(NCS)_2]$ and $[Mn{-}t\mathrm{Bu}_3\text{-}terpy)_2(N_3)_2]$.[5d–e,8]

Reasonable agreement between the experimental and the calculated zfs parameters is found in terms of the absolute value of D even though, as it was already observed, for Mn^{II} compounds, the calculated magnitudes are generally overestimated compared to experimental ones.[7,8] Concerning compounds **2** and **3**, it was recently proposed that the electron donating character of substituents on terpy ligands can induce the increase of the magnitude of D.[5g] However, the calculated contributions of D and especially its D_{SOC} part (SOC: spin-orbit coupling), which is markedly different for both complexes, prevent an interpretation for the observed increase of D between **3** and **2**.

The comparison of the theoretical D values between the 5 and 6 coordinate complexes confirms the experimental data; N5 systems have the largest D value. This seems to be correlated to the D_{SOC}/D_{SS} (SS: spin–spin interaction) ratio, which is noticeably smaller in the case of N6 compounds.

Model study: Our aim is to describe the different contributions to D as a function of the geometry (five versus six coordinate) and the nature of the ligands (N versus O). Therefore, we have developed theoretical models that are the easiest to handle, namely $[Mn(NH_3)_x(OH_2)_y]$ with $x+y=5$ or 6, leading to a total of thirteen structures (labeled $\mathbf{MN^xO^y}$, with $x+y=5$ or 6). Our objectives were i) to analyze the individual contributions of the SOC and SS interactions to D, ii) to compare D as a function of the coordination number of the Mn^{II} ion and iii) to study the influence of nitrogen- versus oxygen-based ligands on D.

We also built two additional models by replacing a water molecule with a hydroxide or a chloride ligand ($\mathbf{MN_5X}$ for $[Mn(NH_3)_5(X)]^+$, X = OH and Cl). These additional calculations were carried out to more directly connect to typical biochemical investigations. If biochemists are studying the structure and/or the reactivity of Mn-containing enzymes, they generally investigate i) the role of the pH to point out the presence of water or hydroxide molecules in the coordination sphere of the Mn^{II} ion and ii) the influence of the addition of anions which present a good affinity to Mn^{II} such as Cl^- (determination of the number of labile ligands and/or the coordination number of the Mn^{II}).

Geometric structure: Geometry optimizations (BP86/TZVP) were performed for all models starting from pseudo-octahedral or trigonal-bipyramidal coordination geometries for six or five coordinate compounds, respectively. The optimized structures of $\mathbf{MN^6}$, $\mathbf{MO^6}$, $\mathbf{MN^5}$ and $\mathbf{MO^5}$ are shown in Figure 5 and detailed metrical parameters obtained for all models are collected in Table 5 and Table 6.

In the five coordinate series, the $\mathbf{MO^5}$ model can be described as a pseudo-trigonal bipyramid as well as a square based pyramid. For all other models, the optimized geometry is best described as a pseudo-trigonal bipyramid with noticeable distortions in the distances between the axial and equatorial ligands, with $Mn{-}L_{ax} > Mn{-}L_{eq}$. As expected, the Mn–N bonds are longer than the Mn–O bonds (Table 5). The optimized bond angles are close to those expected for a perfect trigonal-bipyramidal geometry with $167 < L_{ax}{-}Mn{-}L_{ax} < 193°$, $107 < L_{eq}{-}Mn{-}L_{eq} < 131°$ and $84 < L_{ax}{-}Mn{-}L_{eq} < 99°$.

Concerning the six coordinate models, in each case only one possible configuration is considered, namely the *trans* geometry for $\mathbf{MN^2O^4}$, the *fac* for $\mathbf{MN^3O^3}$ and the *cis* for $\mathbf{MN^4O^2}$. The results obtained for the other configurations

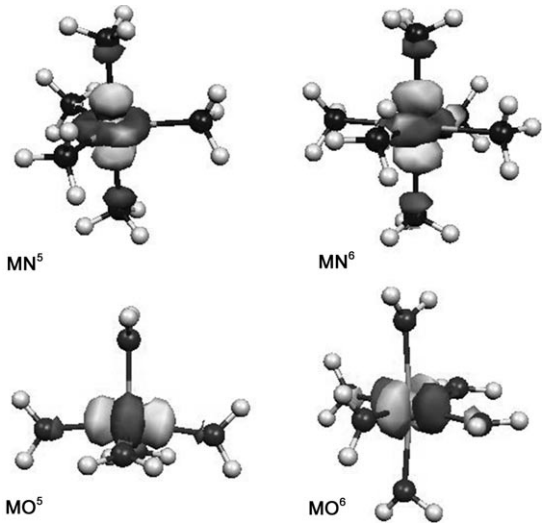

Figure 5. Representation of the **MN^5**, **MO^5**, **MN^6** and **MO^6** models. The d_{z^2} orbital is represented for **MN^5** and **MN^6** and $d_{x^2-y^2}$ for **MO^5** and **MO^6**.

Table 5. Calculated metrical parameters [Å] obtained from the optimized geometry of the five coordinate **MN^xO^y** ($x+y=5$) models. The distances corresponding to the apical bonds are notified with the sign*.

	MN^5	MN^4O^1	MN^3O^2	MN^2O^3	MN^1O^4	MO^5
Mn–X1[a]	2.316*	2.284*	2.269*	2.237*	2.192	2.175*
Mn–X2[a]	2.314*	2.275*	2.217	2.203	2.203*	2.170*
Mn–X3[a]	2.253	2.251	2.213	2.206*	2.189*	2.125
Mn–X4[a]	2.251	2.243	2.275*	2.179	2.154	2.124
Mn–X5[a]	2.247	2.198	2.150	2.148	2.124	2.123

[a] X1 = N for MN^5–MN^1O^4, O for MO^5, X2 = N for MN^5–MN^2O^3, O for MN^1O^4–MO^5, X3 = N for MN^5–MN^3O^2, O for MN^2O^3–MO^5, X4 = N for MN^5–MN^4O^1, O for MN^3O^2–MO^5, X5 = N for MN^5, O for MN^4O^1–MO^5.

are not detailed here, as they bring nothing new to the discussion (the effects of the N versus O ligands). In all models, the Mn^{II} ion is in the center of a distorted octahedron with very small differences in the lengths of the Mn–N and Mn–O bonds in each model (less than 0.04 Å) leading to only small distortions (Table 6). The Mn–N and Mn–O bond distances fall in the ranges between 2.36–2.24 Å and 2.34–2.20 Å, respectively. The octahedral angles are calculated between 165 and 195° along the three axes and 79 and 98° for the others. For the **MN_5X** models, the octahedron is more distorted in **MN_5OH** with angles comprised between 72 and 106° compared to **MN_5Cl** (83–97°).

Electronic structure: Before determining the zfs parameters, we have performed an analysis of the ligand field of the Mn^{II} ion by DFT calculations to better understand the electronic structure of the models. This investigation has been performed by using the set of quasi-restricted molecular orbitals (QRMOs),[13] as we have successfully used this approach in various previous studies.[7,14] In particularly, we have employed the five SOMOs for defining the energy diagram of these metal d-based MOs displayed in Figure 6 and Figure 7.

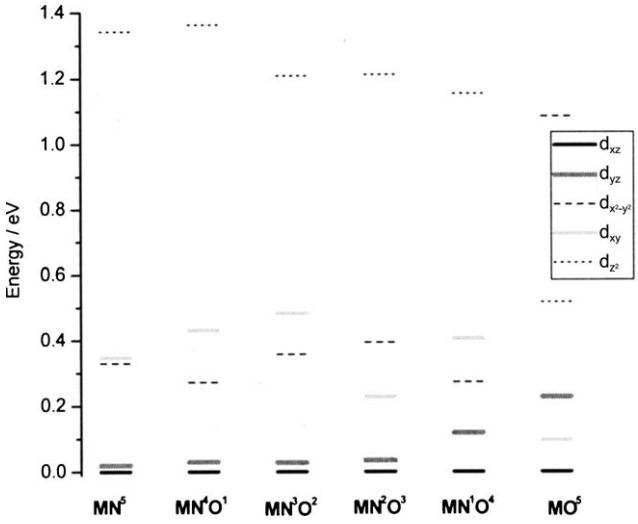

Figure 6. Energy diagrams obtained from the calculated energy (eV) of the quasi restricted SOMOs (top) for the **MN^xO^y** ($x+y=5$) models.

For all five coordinate models except **MO^5**, the resulting schemes are in agreement with an essentially trigonal-bipyramidal geometry (Figure 6). By contrast, the **MO^5** model presents a different scheme, typical of a pseudo C_{4V} symmetry, corresponding to a square based pyramid. This is well reproduced by the QRO energy diagrams. For the trigonal-bipyramidal geometry, the d_{z^2} orbital is the most destabilized one. As expected for almost regular trigonal-bipyramidal coordination geometries, the energy difference between the $d_{x^2-y^2}$ and d_{xy} orbitals and the d_{xz} and d_{yz} ones is very small, the two later being the lowest in energy. The unexpected difference in terms of electronic structure between the **MO^5** and **MN^5** models can be easily rationalized by π interactions originating from the axial water molecule that are obviously not

Table 6. Calculated metrical parameters [Å] obtained from the optimized geometry of the six coordinate **MN^xO^y** ($x+y=6$) and **MN_5X** models. The distances corresponding to the axial bonds are notified with the sign *.

	MN_5OH	MN_5Cl	MN^6	MN^5O^1	MN^4O^2	MN^3O^3	MN^2O^4	MN^1O^5	MO^6
Mn–X1[a]	2.411	2.343	2.355	2.328*	2.320	2.265	2.259	2.241	2.204
Mn–X2[a]	2.362	2.339	2.354	2.328	2.303	2.260*	2.251	2.230	2.203
Mn–X3[a]	2.249	2.338	2.353	2.322	2.295	2.260*	2.249	2.221	2.202
Mn–X4[a]	2.335	2.335	2.352	2.319	2.287	2.302	2.246	2.220*	2.201
Mn–X5[a]	2.295*	2.302*	2.350*	2.319	2.319	2.300	2.240*	2.220*	2.201*
Mn–X6[a]	2.024*	2.475*	2.350*	2.338*	2.290	2.289	2.237*	2.217	2.200*

[a] X1 = N for MN_5X, MN^6–MN^1O^5, O for MO^6, X2 = N for MN_5X, MN^6–MN^2O^4, O for MN^1O^5–MO^6, X3 = N for MN_5X, MN^6–MN^3O^3, O for MN^2O^4–MO^6, X4 = N for MN_5X, MN^6–MN^4O^2, O for MN^3O^3–MO^6, X5 = N for MN_5X, MN^6–MN^5O^1, O for MN^4O^2–MO^6 and X6 = N for MN^6, O for MN_5OH, MN^5O^1–MO^6, Cl for MN_5Cl.

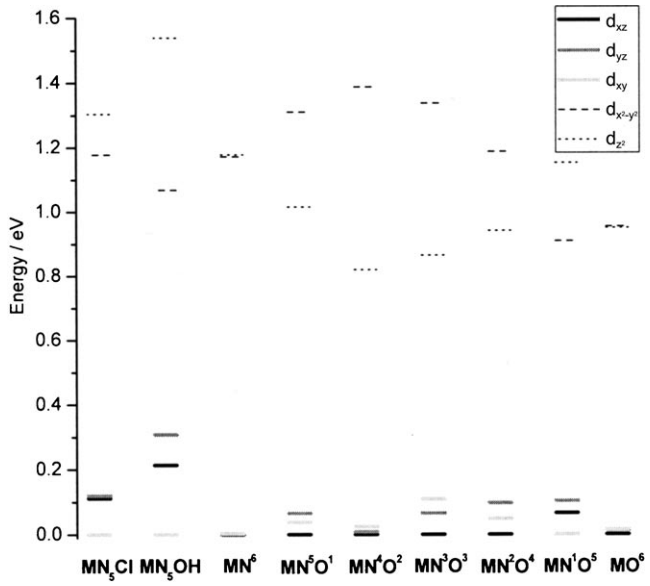

Figure 7. Energy diagrams obtained from the calculated energy (eV) of the quasi restricted SOMOs for the $\mathbf{MN^xO^y}$ ($x+y=6$) and **MX** (X = OH, Cl) models.

present with ammonia ligands. This leads to the destabilization of the $d_{x^2-y^2}$ compared to the d_{z^2} orbitals, the three other d-based MOs remaining quasi-degenerate.

We have also determined the contribution of the manganese atom in the singly occupied MOs of the quasi-restricted MOs (Table 7). For the five models characterized by pseudo-D_{3h} symmetry, we observed an increase of the metal d-character percentage within the anti-bonding orbitals. The anti-bonding interactions with the axial ligands along z explain the strong σ-bond strength of the d_{z^2} orbital. The anti-bonding character is most pronounced for the $d_{x^2-y^2}$ orbital in the $\mathbf{MO^5}$ model. The percentage found for the d_{z^2} orbital agrees with anti-bonding interactions with the basal ligands. Finally, no general trend can be found within the five coordinate series.

Table 7. Percentage of contribution of the manganese of the singly occupied MOs of the $\mathbf{MN^xO^y}$ ($x+y=5$) models from a Löwdin analysis of the quasi-restricted MOs.

	MN^5	MN^4O^1	MN^3O^2	MN^2O^3	MN^1O^4	MO^5
d_{xz}	98.6	98.4	98.4	97.9	97.9	97.6
d_{yz}	98.7	98.5	98.2	97.8	97.3	94.7
$d_{x^2-y^2}$	92.2	93.6	92.8	92.5	94.1	90.8
d_{xy}	92.1	92.4	92.0	94.0	94.1	96.0
d_{z^2}	87.3	87.0	88.5	88.3	89.8	92.2

In the case of the six coordinate models, the energy diagrams agree with an octahedral geometry with the splitting of the d orbitals into e_g and t_{2g} orbitals (Figure 7). For the nearly perfect octahedra $\mathbf{MN^6}$ and $\mathbf{MO^6}$, the e_g and t_{2g} orbitals are close to two- and threefold degeneracy, respectively. In the other models, the distortions originating from the presence of two types of ligands in the coordination sphere lift this quasi-degeneracy.

The determination of the contribution of the manganese atom in the singly occupied MOs of the quasi-restricted MOs correlates well with the QRO energy diagrams (Table 8). The percentage of ligand character increases as a function of the anti-bonding character of the orbital. In the $\mathbf{MN^xO^y}$ ($x+y=6$) series, a noticeable decrease of the σ-bond strength is observed from $x=6$ to 0, although the π-covalency character is comparable in each model. As expected, the presence of a Cl^- or OH^- ligand in the coordination sphere of Mn^{II} increases the σ-bond strength as well as the π-bonding character. This is particularly true if we compare $\mathbf{MN_5OH}$ and $\mathbf{MO^6}$, with a noticeable increase of the two σ- and π-bonding characters in $\mathbf{MN_5OH}$. The increase in the σ-bond strength is well reflected in the orbital splitting of the e_g orbitals in Figure 7.

Calculations of EPR parameters: The EPR parameters of the models were calculated using spin-unrestricted DFT on the BP86 level with the spin-orbit mean field (SOMF)[15] representation of the SOC operator in the implementation.[16] The SOC contribution of D was estimated from the Pederson–Khanna formalism,[17] although for the spin–spin interaction (SS) contribution we have used our recent implementation.[18] The final D-values and its breakdown into individual contributions as well as the E/D are displayed in Table 9 (the manganese isotropic hyperfine and the isotropic g-value are given in the Table S1).

Concerning the isotropic ^{55}Mn-hyperfine coupling, no trend can be found in the series of models and their values are in the expected range (between $\tilde{\nu}=-119$ and -155 MHz).[4–5] The calculated isotropic g-values are close to g_e as expected for ^{6}S-ions except for $\mathbf{MN_5Cl}$ ($g_{iso}=2.0029$). This is in agreement with the contribution of the SOC constant of the chloride anion.[7]

Table 8. Percentage of contribution of the manganese of the singly occupied MOs of the $\mathbf{MN^xO^y}$ ($x+y=6$) and $\mathbf{MN_5X}$ models from a Löwdin analysis of the quasi-restricted MOs.

	MN_5OH	MN_5Cl	MN^6	MN^5O^1	MN^4O^2	MN^3O^3	MN^2O^4	MN^1O^5	MO^6
d_{xz}	96.8	97.6	98.6	98.4	98.4	98.4	97.6	97.7	97.6
d_{yz}	95.9	97.7	98.6	97.6	98.5	98.2	97.9	97.6	97.8
d_{xy}	98.6	98.5	98.7	97.4	97.3	98.0	98.0	98.0	97.3
d_{z^2}	86.4	86.9	89.3	90.3	91.4	91.7	91.4	89.7	91.5
$d_{x^2-y^2}$	90.3	89.5	88.3	88.5	87.7	87.7	89.2	92.2	91.5

D-parameter in five coordinate models: The D parameters calculated for the five coordinate models are underestimated compared to the few experimental data available (Table 4 and Table 10). We found D values between 0.089 and 0.188 cm^{-1}, whereas in synthetic complexes they are close to

Table 9. Calculated zero-field-splitting parameters and the D contributions [cm^{-1}] for the MN^xO^y ($x+y=5$ and 6) and MN_5X models.

	D	D_{SOC}[a]	$\alpha\rightarrow\alpha$[b]	$\beta\rightarrow\beta$[b]	$\alpha\rightarrow\beta$[b]	$\beta\rightarrow\alpha$[b]	D_{SS}[c]	1-center[d]	2-center[d] (coulomb)	2-center[d] (hybrid)	3-center[d] (coulomb)	E	E/D[e]
MN^5	−0.188	−0.183	−0.025	0.005	−0.133	−0.029	−0.005	−0.002	−0.009	+0.003	+0.003	−0.009	0.048
MN^4O^1	−0.130	−0.155	−0.013	+0.009	−0.131	−0.020	+0.025	+0.016	0	+0.009	+0.001	−0.010	0.078
MN^3O^2	−0.162	−0.141	−0.026	−0.005	−0.092	−0.018	−0.021	−0.009	−0.009	−0.007	+0.003	−0.026	0.133
MN^2O^3	−0.104	−0.121	−0.013	+0.007	−0.100	−0.016	+0.017	+0.010	−0.002	+0.007	+0.001	−0.015	0.141
MN^1O^4	−0.148	−0.118	−0.027	−0.006	−0.070	−0.016	−0.030	−0.017	−0.012	−0.005	+0.004	−0.026	0.179
MO^5	−0.089	−0.089	−0.017	−0.004	−0.060	−0.009	0	0	0	0	0	−0.005	0.048
MN^6	+0.030	0	0	0	0	0	+0.030	+0.024	+0.006	+0.002	−0.002	0	0.005
MN^5O^1	+0.018	−0.012	+0.005	+0.004	−0.021	0	+0.031	+0.017	+0.006	+0.009	−0.002	+0.006	0.302
MN^4O^2	+0.015	+0.001	−0.002	−0.002	+0.003	+0.001	+0.014	+0.014	+0.001	−0.002	+0.001	+0.003	0.174
MN^3O^3	+0.030	−0.019	0.020	0.018	−0.055	−0.002	+0.050	+0.008	+0.012	+0.033	−0.004	+0.004	0.131
MN^2O^4	+0.017	−0.030	+0.011	+0.011	−0.052	0	+0.048	+0.018	+0.010	+0.023	−0.003	+0.003	0.184
MN^1O^5	+0.028	−0.007	+0.015	+0.014	−0.035	−0.001	+0.035	+0.008	+0.009	+0.020	−0.003	+0.005	0.190
MO^6	+0.025	−0.003	0.0010	0.008	−0.018	−0.003	+0.029	+0.035	−0.002	−0.006	+0.003	0	0.006
MN_5Cl	+0.113	+0.089	0.028	0.058	0.015	−0.012	+0.025	−0.004	+0.003	+0.031	−0.005	+0.006	0.054
MN_5OH	+0.057	−0.003	0.016	0.019	−0.042	0.004	+0.059	+0.046	−0.008	+0.017	+0.005	+0.003	0.062

[a] the SOC contribution to the total D value; [b] the excitations contributing to the total D_{SOC} value, [c] the SS contribution to the total D value; [d] the n-center contributions to the total D_{SS} value; [e] no unit.

Table 10. Experimental D values and coordination number of five and six coordinate mononuclear Mn^{II} complexes. The D sign has been specified when it is known.

	D [cm^{-1}]	Coord. Number	Ref.		D [cm^{-1}]	Coord. Number	Ref.
FosA + fosfomycin	0.235	5	[4b]	FosA	0.060	6	[4a]
Mn−superoxide dismutase *E. coli*	0.355	5	[4c]	Mn−superoxide dismutase *E. Coli* $+N_3^-$	0.046	6	[4c]
[Mn(tBu$_3$-terpy)(N_3)$_2$]	−0.250	5	[5e]	Mn^{II} concanavalin A	0.022	6	[4g]
[Mn(terpy)(NCS)$_2$]	−0.300	5	[5d]	Mn^{II} -substituted xylose isomerase	0.036	6	[2b]
[Mn(tpa)(NCS)$_2$] (**1**)	−0.085	6	this work	$[Mn(OH_2)_6]^{2+}$	0.018	6	[4e]
$[Mn(terpy)_2]^{2+}$ (**3**)	−0.042	6	this work	Mn^{II} ATP	0.035	6	[4e]
$[Mn(tBu_3\text{-}terpy)_2]^{2+}$ (**2**)	−0.073	6	this work				

0.30 cm^{-1} and in enzymes between 0.23 and 0.36 cm^{-1}. The use of simplified ligands (ammonia and/or aqua ligands) is certainly responsible of the origin of this underestimation since the D-values calculated from the crystal structure of the synthetic complexes are, if anything, overestimated by the present methodology.

The SS contribution represents from 0 to 20% of the total D-values in the models while for the synthetic complexes the SS part is far from being negligible (about 35%) (Table 9). The major part of D arises from the SOC contribution with a noticeable trend: the D_{SOC} decreases when the number of water ligands increases (from 0.183 for **MN^5** to 0.089 for **MO^5**).

Given that in halide Mn^{II} complexes the spin-orbit coupling of the halide ion contributes in an essential way to the final D-value, we have explored the relative contributions of the ligands versus the manganese SOC to D. These calculations have been performed using the effective nuclear charge model developed by Koseki et al.[18] to replace the SOMF operator (Experimental Section). The results obtained for the two extreme cases (**MN^5** and **MO^5**) are reported in Table 11.

With the Z_{eff} representation, the total D value is slightly lower than with the SOMF approach (less than 20%). Because the difference between these two methods is the treatment of the SOC operator, the D_{SS} part is identical. The results unambiguously show that the manganese SOC exclusively contributes to D_{SOC} in the present series.

Table 11. Calculated electronic parameters D, D_{SOC} and D_{SS} (cm^{-1}) and the contributions to the D_{SOC} for the **MN^5** and **MO^5**. Models in three cases: (total); Z_{eff} with their default values for all atoms, and Z_{eff} set to zero for either Mn (no Mn_{SOC}) or the coordinated atom (no N_{SOC} or no O_{SOC}).

	MN^5			**MO^5**		
	Total	no Mn_{SOC}	no N_{SOC}	Total	no Mn_{SOC}	no O_{SOC}
D^{SOMF}	−0.183			−0.089		
$D^{Z_{eff}}$	−0.145	−0.024	−0.146	−0.069	+0.031	−0.065
D_{SS}	−0.005	−0.024	−0.005	0	+0.031	0
D_{SOC}	−0.139	0	−0.141	−0.069	0	−0.066
$\alpha\rightarrow\alpha$	−0.018	0	−0.017	−0.012	0	−0.009
$\beta\rightarrow\beta$	+0.002	0	+0.003	−0.005	0	0
$\alpha\rightarrow\beta$	−0.113	0	−0.115	−0.051	0	−0.052
$\beta\rightarrow\alpha$	−0.011	0	−0.011	−0.002	0	−0.004

As detailed in the Experimental Section, four transitions contribute to the D_{SOC} part. The $\alpha\rightarrow\beta$ class, on which ligand field theory focuses for high-spin d^5 ions, represents the most important contribution (from 60 to 85% of D_{SOC}) which still follows the trend found within the series. Never-

theless, even if the D_{SS} part is minor, its contribution disturbs this tendency. Compared to our previous results mainly obtained for five and six coordinate halide Mn^{II} complexes, the relative ratio between the four excitation class contributions is different.[7–8] In halide systems the four transitions present similar magnitudes with opposite sign. In contrast, for the $\mathbf{MN^xO^y}$ ($x+y=5$) models, the main contribution is $D_{\alpha\beta}$ and no trend is found concerning the sign and the relative magnitude of the other contributions.

The D-parameter in six coordinate models: The D parameters found for the $\mathbf{MN^xO^y}$ ($x+y=6$) series fall into the narrow range from 0.014 to 0.030 cm^{-1} (Table 9). The D value found for $\mathbf{MO^6}$ is in very good agreement with the experimental data (Table 10), demonstrating once more the validity of our approach. All other synthetic or biological complexes display larger D-values, telling us that the complexity of the ligands slightly increases the zfs (comprised between 0.022 and 0.105 cm^{-1}) as for the five coordinate models (see below). The very small E-value prevents any exploitation of this parameter as well as E/D. However, we note that for $\mathbf{MN^6}$ and $\mathbf{MO^6}$, E/D is close to zero in agreement with their structure and their energy diagram.

The quantification of both D contributions (D_{SOC} and D_{SS}) unambiguously reveals that the major part of D arises from the SS interaction (more than 75%). Even if it less pronounced (more than 60%), the same is also observed for the synthetic complexes. While for $\mathbf{MN^6}$ D_{SOC} is equal to zero, in the other models, the small D_{SOC} values are of opposite sign than D_{SS}. As for D, no discernible trend is found for D_{SS} along the series.

The replacement of a water or ammonia ligand by a hydroxide or chloride leads to an apparent increase of D (0.057 and 0.113 cm^{-1}, respectively). However, whereas the major contribution for $\mathbf{MN_5OH}$ originates from the SS interaction, the SOC part represents about 80% of D in $\mathbf{MN_5Cl}$. This agrees with our previous results, which demonstrate that the D value of halide Mn^{II} compounds mainly originates from the D_{SOC} contribution and more particularly is proportional to a mixing term between the SOC of the manganese and the halide ligand. The deprotonation of a water ligand leads to an increase of D, only originating from the SS contribution, because D_{SOC} has the same value in $\mathbf{MN_5OH}$ and $\mathbf{MO_6}$.

Discussion

Magneto-structural correlations can be proposed from experimental observations, but need to be supported by an understanding of their physical origins. This last crucial point requires a theoretical method that is suitable for the studied systems. For the Mn^{II} ion, although EPR spectroscopy is the most appropriate tool for experimentally determining the zfs parameters, we have recently shown that DFT is an adequate approach for the investigation of a number of Mn^{II} complexes.[7,8] Indeed, the complementarity of both methods allowed a qualitative and quantitative determination of the different contributions to the D value. The principal results were that i) D_{SS} is negligible for the iodide and bromide complexes and starts to be significant for the chloride compounds; ii) D_{SOC}, the main contribution to D, corresponds to the addition of four contributions characterized by comparable magnitudes and opposite signs and iii) the origin of D_{SOC} arises from interference between the metal- and halide-SOC contributions, proportional to the SOC of the manganese and the halide. This theoretical investigation thus established that D is governed by the nature of the halide and not primarily by the coordination number of the Mn^{II} ion. The magnitude of D is between 0.9 and 1.2 cm^{-1} for the iodo complexes, 0.5 and 0.7 cm^{-1} for the bromo, and 0.16 and 0.30 cm^{-1} for the chloro-derivatives,[5a,c,d,f] except for the *cis* dihalide six coordinate systems,[5b,7] which are characterized by significantly lower D values ($|D_I|=0.6$ cm^{-1}, $|D_{Br}|=0.35$ cm^{-1}, $|D_{Cl}|=0.12$ cm^{-1}).

In the present work, our purpose is different, as we focus on mononuclear Mn^{II} complexes characterized by a coordination sphere typically found in biological systems with only nitrogen (amine or imine) and/or oxygen (alcohol or carboxylate) based ligands. Based on a few experimental results, it was proposed for such Mn^{II} complexes that D is correlated with the coordination number: D values larger than 0.2 cm^{-1} are assigned to five coordinate systems, whereas D values smaller than 0.11 cm^{-1} correspond to six coordinate compounds (Table 4 and Table 10).[4a,c]

However, this correlation is apparently contradicted for one compound, a N6 Mn^{II} complex magnetically diluted in a Zn or a Cd matrix, $[M(Mn)(bpa)_2]^{2+}$ (M = Cd or Zn; bpa = *N,N*-bis(2-pyridylmethyl)-amine).[19] The magnitudes of D found are actually larger than 0.11 cm^{-1} (-0.175 and -0.219 cm^{-1} in $[Cd(Mn)(bpa)_2]^{2+}$ and $[Zn(Mn)(bpa)_2]^{2+}$, respectively).[19] Nevertheless, the D value has never been determined on the neat powder of $[Mn(bpa)_2]^{2+}$ in order to confirm the large D values found with the diluted samples. In order to clarify this point, we have recorded the X-band EPR spectrum of a very similar compound: $[Mn(bpea)_2]^{2+}$ (bpea = *N,N*-bis(2-pyridylmethyl)-ethylamine). The experimental D-value is found around 0.08 cm^{-1}, noticeably smaller than the values found for $[M(Mn)(bpa)_2]^{2+}$ and is in the range expected for such six coordinate complexes. We also performed DFT calculations from the available X-ray structures of $[Mn(bpea)_2]^{2+}$[20] and $[Mn(bpa)_2]^{2+}$[19] and found comparable D values ($D=-0.079$ and -0.087 cm^{-1}, respectively). These results show that the Mn^{II} compound magnetically diluted in the Zn and Cd matrix is different from the $[Mn(bpa)_2]^{2+}$ complex.

Therefore, from an experimental point of view, for all structurally well characterized Mn^{II} complexes with only nitrogen or oxygen based ligands, D seems to be clearly correlated with the coordination number of the Mn^{II} ion. This is strongly supported by our theoretical investigation. Interestingly the origins of D are different in five or six coordinate systems implying contributions, which differ in their nature and magnitude. For five coordinate systems, the major part of D corresponds to D_{SOC} and more precisely to the α,β

transitions. On the other hand, for six coordinate systems, the main contribution to D arises from D_{SS}.

The theoretical models with ammonia or aqua ligands as well as $[Mn(OH_2)_6]^{2+}$ lead to smaller D values compared to the synthetic or biological Mn^{II} complexes with comparable coordination sphere. The larger values can be attributed to the electronic effects or geometric constraints generated by the intricate ligands. Work is in progress to understand this difference.

How can this investigation help to predict the structure of an active site in metalloenzymes? It is now unambiguous that by HF-EPR, a precise measure of D will lead to the coordination number of the Mn^{II} site. The determination of the number of labile ligands in the coordination sphere is generally performed by the addition of chloride anion(s). If the active site is initially six coordinate, a ligand exchange with Cl^- will induce a noticeable increase of D ($D < 0.10$ and $D > 0.12\ cm^{-1}$ without or with Cl, respectively). From a five coordinate complex, the addition of Cl^- will lead to a six coordinate system (Cl^- addition) or to a five coordinate one (a ligand exchange) resulting to comparable D values. Therefore, HF-EPR experiments will be appropriate for studying the number of labile ligands in the coordination sphere of a Mn^{II} site only in the case of six coordinate systems.

The deprotonation of a water ligand seems to induce an increase of D but this theoretical study needs to be supported by experimental data. Furthermore, from our theoretical results, the nature of the ligands N versus O can not be predicted since the relative ratio of the number of ammonia over aqua ligands has no evident effect on the D value. This requests to be experimentally confirmed. If mononuclear Mn^{II} complexes with nitrogen based ligands comprised of amine or imine functions are largely available, there is lack of studies performed on compounds with oxygen based ligands especially carboxylate ones. Our future objective is the synthesis and investigation of six coordinate compounds with carboxylate anions in different coordination modes.

Conclusion

Finally, our studies demonstrate the scope, but also the complexity of defining general magneto-structural correlations for a particular metal ion. This complete investigation together with our previous works leads us to understand the factors that control the magnitudes in the zfs parameters for five- versus six-coordinate Mn^{II} complexes and to propose clear correlations for the Mn^{II} ion. According to our results, we propose to categorize Mn^{II} complexes into two classes: class 1 contains halide anions for which D is correlated with the nature of the halide and class 2 for which the D values are intimately linked to the coordination number. This work evidenced that combining experimental and theoretical approaches is fruitful and needs to be further developed for other metals and oxidation states. Work along these lines is in progress in our laboratories.

Experimental Section

General: Reagents and solvents (analytical grade) were purchased from Aldrich and Fluka and used as received. Tris-2-picolylamine or tris(2-pyridylmethyl)amine (tpa) was prepared according to the literature method.[21] 4,4′,4″-tri-tert-butyl-2,2′:6′,2″-terpyridine (tBu$_3$-terpy) was purchased from Aldrich. The complexes $[Mn(terpy)_2](I)_2$ **(3)** (terpy = 2,2′:6′,2″-terpyridine) and $[Mn(bpea)_2](PF_6)_2$ (bpea = N,N-bis(2-pyridylmethyl)-ethylamine) were prepared as previously described.[9,20,22] Elemental analysis were performed by the Service Central d′Analyse du CNRS at Vernaison (France).

Synthesis of [Mn(tpa)(NCS)$_2$] (1): To a stirred solution of tpa (82.7 mg, 0.284 mmol) in methanol (3 mL) was added $Mn(NO_3)_2{\cdot}4H_2O$ (71.4 mg, 0.284 mmol). Addition of a methanolic solution (4 mL) of KNCS (57.1 mg, 0.587 mmol) yielded a white precipitate, which was filtered off and redissolved in CH_3CN. Colorless crystals of **1**·CH_3CN were obtained at room temperature by diffusion of ethyl acetate into the CH_3CN solution. Yield: 0.121 g (80 %). IR (KBr) $\tilde{\nu}$ = 3451 (vs), 2057 (vs), 1602 (s), 1573 (m), 1482 (m), 1439 (s), 1393 (w), 1384 (w), 1373 (w), 1351 (w), 1351 (w), 1325 (w), 1311 (w), 1290 (m), 1269 (w), 1245 (w), 1153 (m), 1121 (m), 1097 (m), 1052 (m), 1016 (m), 996 (w), 976 (w), 957 (w), 906 (w), 883 (w), 855 (w), 807 (w), 766 (s), 758 (s), 639 (m), 508 (w), 481(w), 416 (m), 317 cm^{-1} (w); elemental analysis calcd (%) for $C_{20}H_{18}MnN_6S_2{\cdot}CH_3CN{\cdot}H_2O$: C 50.76, H 4.45, N 18.83, S 12.32; found: C 50.77, H 4.04, N 18.05, S 12.50.

Synthesis of [Mn(tBu$_3$-terpy)$_2$](PF$_6$)$_2$ (2): To a solution of anhydrous $MnCl_2$ (0.031 g, 0.248 mmol) in ethanol (30 mL) was added tBu$_3$-terpy (0.200 g, 0.498 mmol) in ethanol (30 mL). The resulting yellow solution was heated at reflux for 1 h. After cooling to room temperature, the addition of saturated aqueous solution of KPF_6 (10 mL) allowed the precipitation of the complex. The yellow solid was redissolved in dichloromethane and washed three times with water. After drying over anhydrous Na_2SO_4, the CH_2Cl_2 was removed under reduced pressure. The precipitate was then reprecipitated from CH_2Cl_2/diethyl ether. Yield: 0.166 g (58 %). IR (KBr): $\tilde{\nu}$ = 3428 (s), 2965 (s), 1610 (s), 1610 (s), 1553 (m), 1485 (m), 1470 (m), 1426 (w), 1404 (m), 1370 (w), 1304 (w), 1253 (m), 1204 (w), 1125 (w), 1015 (m), 918 (w), 903 (w), 838 (vs), 744 (w), 731 (w), 698 (w), 670 (w), 613 (m), 557 (s), 461 cm^{-1} (w). Single yellow crystals of [Mn(tBu$_3$-terpy)$_2$](PF$_6$)$_2{\cdot}C_4H_{10}O{\cdot}0.5\,C_2H_5OH{\cdot}0.5\,CH_3OH$ were obtained by slow vapor diffusion of diethyl ether in a concentrated solution of **2** in a mixture of methanol and ethanol.

Synthesis of [Zn(Mn)(tolyl-terpy)$_2$](PF$_6$)$_2$: To a stirred solution of terpy (96.3 mg, 0.413 mmol) in acetone (4–5 mL) was added a water solution (6 mL) of $Mn(OAc)_2{\cdot}4H_2O$ (1.1 mg (2 %), 0.0044 mmol) and $Zn(OAc)_2$ (37.1 mg (98 %), 0.2022 mmol). The resulting solution was stirred for 10 min. Addition of a saturated aqueous KPF_6 solution (3 mL) yielded a yellow precipitate, which was filtered, washed with small amount of ethanol, and dried in vacuo. Yield: 0.135 g (79 %). IR (KBr) $\tilde{\nu}$ = 3132 (m), 1601 (s), 1583 (m), 1565 (m), 1479 (s), 1455 (s), 1438 (s), 1414 (w), 1324 (s), 1300 (w), 1248 (m), 1195 (m), 1163 (s), 1107 (w), 1052 (w), 1030 (m), 1014 (s), 978 (w), 927 (m), 903 (m), 839 (vs), 825 (vs), 771 (vs), 741 (w), 728 (w), 651 (m), 638 (m), 558 (vs), 516 (w), 428 (m), 403 cm^{-1} (w).

Physical measurements: IR spectra were obtained by using a Perkin–Elmer Spectrum GX spectrophotometer, controlled by a Dell Optiplex GXa computer. Spectra were recorded from a solid sample at 1 % by mass in a pellet of KBr. High-frequency and high-field EPR spectra were recorded by means of a laboratory made spectrometer[23] by using powder samples pressed in pellets to avoid preferential orientation of the crystallites in the strong magnetic field. Gunn diodes operating at $\tilde{\nu}$ = 95 GHz and 115 GHz and equipped with a second- and third-harmonic generator have been used as the radiation source. The magnetic field was produced by a superconducting magnet (0–12 T). The simulation of the HF-EPR spectra was performed by using the SIM program written by H. Weihe.[5a]

Crystal structure determination: Diffraction data were collected by using a Bruker SMART diffractometer with $Mo_{K\alpha}$ radiation. Crystal of complexes of dimensions $0.5 \times 0.15 \times 0.15$ mm for **1**·CH_3CN, $0.50 \times 0.40 \times$

0.08 mm for **2**·$C_4H_{10}O$·0.5 C_2H_5OH·0.5 CH_3OH were selected. The crystallographic data are summarized in Tables 1–3. All calculations were effected using the SHELXTL computer program.[24] CCDC 610222 (**1**) and 679394 (**2**) contain the supplementary crystallographic data for this paper. These data can be obtained free of charge from The Cambridge Crystallographic Data Centre via www.ccdc.cam.ac.uk/data_request/cif. **Theoretical calculations**: All calculations reported in this work were performed with the ORCA program package.[25] The structure of the models $[Mn^{II}(NH_3)_x(OH_2)_y]$ ($x+y=5$ or 6) were fully optimized by using the BP86 functional[26] and the TZVP basis set.[27] Two physical factors have been taking into account for the DFT calculation of the zfs: the electron–electron magnetic dipolar spin–spin interaction (SS) and the spin-orbit coupling (SOC) of excited states into the ground state.[13a] EPR properties were calculated by using spin-unrestricted DFT together with both the spin-orbit mean field (SOMF) representation[15] of the spin-orbit coupling (SOC) operator in the implementation of ref[16] as well as the effective nuclear charge SOC-Hamiltonian parameterized by Koseki et al.[18] In the latter, the SOC is represented by a sum over atomic contributions [Eq. (2)]:

$$\hat{H}_{\mathrm{SOC}} = \frac{\alpha^2}{2} \sum_i \sum_A \frac{Z_A^{\mathrm{eff}}}{|r_i - R_A|^3} \hat{\mathbf{l}}_{iA} \hat{\mathbf{s}}_i \tag{2}$$

In wich α is the fine-structure constant ($\approx 1/137$ in atomic units), i sums over electrons and A over atoms; r_i is the position of the i^{th} electron and R_A the position of nucleus A. The operators $\hat{\mathbf{s}}_i$ and $\hat{\mathbf{l}}_{iA}$ represent the spin of the i^{th} electron and its angular momentum relative to atom A respectively. Z_A^{eff} is a semi-empirically chosen effective nuclear charge that is generally smaller than the true nuclear charge Z_A in order to compensate for the neglect of two-electron terms that essentially provide a screening. For the calculation of the spin–spin contribution to the zfs we refer to Ref. [13a] whereas the SOC contribution was calculated with the method of Pederson and Khanna[17] to allow for easier comparison with the work of other authors that have implemented the same methodology. A forthcoming paper will compare this approach with the recently developed coupled-perturbed SOC method for the treatment of the SOC contribution.[28] In this work, the SS and SOC contributions to the D-tensor are calculated as [Eq. (3) and (4)]:

$$D_{kl}^{(\mathrm{SS})} = \frac{g_e^2}{4} \frac{\alpha^2}{S(2S-1)} \cdot \sum_{\mu\nu} \sum_{\kappa\tau} \{P_{\mu\nu}^{\alpha-\beta} P_{\kappa\tau}^{\alpha-\beta} - P_{\mu\kappa}^{\alpha-\beta} P_{\nu\tau}^{\alpha-\beta}\} \langle \mu\nu | r_{12}^{-5} \{3 r_{12,k} r_{12,l} - \delta_{kl} r_{12}^2\} | \kappa\tau \rangle \tag{3}$$

$$\begin{aligned} D_{KL}^{(\mathrm{SOC})} = & -\frac{1}{4S^2} \sum_{i_\beta, a_\beta} \frac{\langle \psi_i^\beta | h_K^{\mathrm{SOC}} | \psi_a^\beta \rangle \langle \psi_a^\beta | h_L^{\mathrm{SOC}} | \psi_i^\beta \rangle}{\varepsilon_a^\beta - \varepsilon_i^\beta} \\ & -\frac{1}{4S^2} \sum_{i_\alpha, a_\alpha} \frac{\langle \psi_i^\alpha | h_K^{\mathrm{SOC}} | \psi_a^\alpha \rangle \langle \psi_a^\alpha | h_L^{\mathrm{SOC}} | \psi_i^\alpha \rangle}{\varepsilon_a^\alpha - \varepsilon_i^\alpha} \\ & +\frac{1}{4S^2} \sum_{i_\alpha, a_\beta} \frac{\langle \psi_i^\alpha | h_K^{\mathrm{SOC}} | \psi_a^\beta \rangle \langle \psi_a^\beta | h_L^{\mathrm{SOC}} | \psi_i^\alpha \rangle}{\varepsilon_a^\beta - \varepsilon_i^\alpha} \\ & +\frac{1}{4S^2} \sum_{i_\beta, a_\alpha} \frac{\langle \psi_i^\alpha | h_K^{\mathrm{SOC}} | \psi_a^\alpha \rangle \langle \psi_a^\alpha | h_L^{\mathrm{SOC}} | \psi_i^\alpha \rangle}{\varepsilon_a^\alpha - \varepsilon_i^\beta} \end{aligned} \tag{4}$$

Here, S is the total spin of the electronic ground state ($^5/_2$ here), $g_e(2.002319\ldots)$ is the free electron g-value, ($\approx 1/137$) the fine structure constant, $P^{\alpha-\beta}$ the spin-density matrix in the atomic orbital basis $\{\varphi_\mu\}$, which is used to expand the molecular spin-orbitals as $\psi_p^\sigma = \Sigma_\mu c_{\mu p}^\sigma \varphi_\mu$ with orbital energies ε_p^σ ($p = i$ and a refers to occupied and unoccupied spin-orbitals respectively). The operator $r_{12}^{-5}\{3 r_{12,k} r_{12,l} - \delta_{kl} r_{12}^2\}$represents the dipolar spin–spin coupling between a pair of electrons and h_K^{SOC} the K'th spatial component of a reduced SOC operator ($K, L = x,y,z$).[16,29]

Four types of excitations contributes to the D_{SOC} part[13a] and in the one-electron approximation take the form: i) excitation of a spin-down (β) electron from a doubly occupied MO (DOMO) to a SOMO leading to states of the same spin S as ground state ($\beta \rightarrow \beta$), ii) the excitation of a spin-up (α) electron from a SOMO to a virtual MO (VMO) also giving rise to states of total spin S ($\alpha \rightarrow \alpha$), iii) excitations between two SOMOs that are accompanied by a spin-flip and giving rise to states of $S' = S-1$ ($\alpha \rightarrow \beta$), and iv) "shell-opening" transitions from a DOMO to a VMO leading to states of $S' = S+1$ ($\beta \rightarrow \alpha$).

Acknowledgements

C.D. and M.-N.C. thank the Agence Nationale pour la Recherche (Grant No. ANR-05-JCJC-0171–01) for financial support. This work was also supported by the bilateral France-Germany Hubert Curien program (Procope 2008–2009).

[1] a) *Metal ions in biological systems: Manganese and its role in biological processes*, vol. 37, (eds.: A. Sigel, H. Sigel) New York, Marcel Dekker **2000** and references therein; b) A.-F. Miller, *Curr. Opin. Chem. Biol.* **2004**, *8*, 162; c) T. A. Jackson, T. C. Brunold, *Acc. Chem. Res.* **2004**, *37*, 461; d) V. V. Barynin, M. M. Whittaker, S. V. Antonyuk, V. S. Lamzin, P. M. Harrison, P. J. Artymiuk, J. W. Whittaker, *Structure* **2001**, *9*, 725; e) K. N. Ferreira, T. M. Iverson, K. Maghlaoui, J. Barber, S. Iwata, *Science* **2004**, *303*, 1831; f) B. Loll, J. Kern, W. Saenger, A. Zouni, J. Biesiadka, *Nature* **2005**, *438*, 1040.

[2] a) C. Buy, G. Girault, J.-L. Zimmermann, *Biochemistry* **1996**, *35*, 9880; b) R. Kappl, K. Ranguelova, B. Koch, C. Duboc, J. Hüttermann, *Magn. Reson. Chem.* **2005**, *43*, S65.

[3] These become significant if the symmetry of the system is so high (cubic) that the quadratic terms vanish. In the much more frequently low-symmetry cases they merely provide minor corrections. Therefore these terms are disregarded in this work. A. Abragam and B. Bleaney in *Electron paramagnetic resonance of transition ions*, Clarendon press, Oxford, **1970**.

[4] a) S. K. Smoukov, J. Telser, B. A. Bernat, C. L. Rife, R. N. Armstrong, B. M. Hoffman, *J. Am. Chem. Soc.* **2002**, *124*, 2318; b) C. J. Walsby, J. Telser, R. E. Rigsby, R. N. Armstrong, B. M. Hoffman, *J. Am. Chem. Soc.* **2005**, *127*, 8310; c) S. Un, P. Dorlet, G. Voyard, L. C. Tabares, N. Cortez, *J. Am. Chem. Soc.* **2001**, *123*, 10123; d) N. Bondarava, S. Un, A. Krieger-Liszkay, *Biochim. Biophys. Acta* **2007**, *1767*, 583; e) T. A. Stich, S. Lahiri, G. Yeagle, M. Dicus, M. Brynda, A. Gunn, C. Aznar, V. J. DeRose, R. D. Britt, *Appl. Magn. Reson.* **2007**, *31*, 321; f) R. Carmieli, P. Manikandan, A. J. Kalb Gilboa, D. Goldfarb, *J. Am. Chem. Soc.* **2001**, *123*, 8378; g) E. Meirovitch, Z. Luz, A. J. Kalb, *J. Am. Chem. Soc.* **1974**, *96*, 7542.

[5] a) C. J. H. Jacobsen, E. Pedersen, J. Villardsen, H. Weihe, *Inorg. Chem.* **1993**, *32*, 1216; b) R. M. Wood, D. M. Stucker, L. M. Jones, W. B. Lynch, S. K. Misra, J. H. Freed, *Inorg. Chem.* **1999**, *38*, 5384; c) D. M. L. Goodgame, H. El Mkami, G. M. Smith, J. P. Zhao, E. J. L. McInnes, *Dalton Trans.* **2003**, 34; d) C. Mantel, Baffert, I. Romero, A. Deronzier, J. Pécaut, M.-N. Collomb, C. Duboc, *Inorg. Chem.* **2004**, *43*, 6455; e) C. Mantel, Philouze, M.-N. Collomb, C. Duboc, *Eur. J. Inorg. Chem.* **2004**, 3880; f) C. Duboc, V. Astier-Perret, H. Chen, J. Pécaut, R. H. Crabtree, G. W. Brudvig, M.-N. Collomb, *Inorg. Chim. Acta* **2006**, *359*, 1541; g) J. Gätchens, M. Sjödin, V. L. Pecoraro, S. Un, *J. Am. Chem. Soc.* **2007**, *129*, 13825.

[6] C. Pichon, P. Mialane, E. Riviere, G. Blain, A. Dolbecq, J. Marrot, F. Secheresse, C. Duboc, *Inorg. Chem.* **2007**, *46*, 7710.

[7] C. Duboc, T. Phoeung, S. Zein, J. Pécaut, M.-N. Collomb, F. Neese, *Inorg. Chem.* **2007**, *46*, 4905.

[8] S. Zein, C. Duboc, W. Lubitz, F. Neese, *Inorg. Chem*, **2007**, *47*, 134.

[9] C. Baffert, I. Romero, J. Pecaut, A. Llobet, A. Deronzier, M.-N. Collomb, *Inorg. Chim. Acta* **2004**, *357*, 3430.

[10] H. Oshio, E. Ino, I. Mogi, I. Ito, *Inorg. Chem.* **1993**, *32*, 5697.

[11] a) J. Limburg, J. S. Vrettos, R. H. Crabtree, G. W. Brudvig, J. C. de Paula, A. K. Hassan, A.-L. Barra, C. Duboc-Toia, M.-N. Collomb, *Inorg. Chem.* **2001**, *40*, 1698; b) C. Mantel, A. K. Hassan, J. Pécaut, A. Deronzier, M.-N. Collomb, C. Duboc-Toia, *J. Am. Chem. Soc.* **2003**, *125*, 12337; c) C. Mantel, H. Chen, R. H. Crabtree, G. W.

Brudvig, J. Pécaut, M.-N. Collomb, C. Duboc, *ChemPhysChem* **2005**, *6*, 541.
[12] C. Duboc, T. Phoeung, D. Jouvenot, A. G. Blackman, L. F. McClintock, J. Pécaut, M.-N. Collomb, A. Deronzier, *Polyhedron* **2007**, *26*, 5243.
[13] a) F. Neese, *J. Am. Chem. Soc.* **2006**, *128*, 10213; b) S. Sinnecker, F. Neese, L. Noodleman, W. Lubitz, *J. Am. Chem. Soc.* **2004**, *126*, 2613.
[14] a) J. Schöneboom, F. Neese, W. Thiel, *J. Am. Chem. Soc.* **2005**, *127*, 5840; b) K. Ray, A. Begum, T. Weyhermüller, S. Piligkos, J. van Slageren, F. Neese, K. Wieghardt, *J. Am. Chem. Soc.* **2005**, *127*, 4403.
[15] B. A. Hess, C. M. Marian, U. Wahlgren, O. Gropen, *Chem. Phys. Lett.* **1996**, *251*, 365.
[16] F. Neese, *J. Chem. Phys.* **2005**, *122*, 034107.
[17] M. R. Pederson, S. N. Khanna, *Phys. Rev.* B **1999**, *60*, 9566.
[18] a) S. Koseki, M. S. Gordon, M. W. Schmidt, N. Matsunaga, *J. Phys. Chem.* **1995**, *99*, 12764; b) S. Koseki, M. W. Schmidt, M. S. Gordon, *J. Phys. Chem. A* **1998**, *102*, 10430.
[19] J. Glerup, P. A. Goodson, D. J. Hodgson, K. Michelsen, K. M. Nielsen, H. Weihe, *Inorg. Chem.* **1992**, *31*, 4611.
[20] I. Romero, L. Dubois, M.-N. Collomb, A. Deronzier, J.-M. Latour, J. Pécaut, *Inorg. Chem.* **2002**, *41*, 1795.
[21] K. D. Karlin, J. C. Hayes, J. P. Hutchinson, J. Zubieta, *Inorg. Chem.* **1982**, *21*, 4106.
[22] M.-N. C. Dunand-Sauthier, A. Deronzier, I. Romero, *J. Electroanal. Chem.* **1997**, *436*, 219.
[23] a) A.-L. Barra, L.-C. Brunel, J. B. Robert, *Chem. Phys. Lett.* **1990**, *165*, 107; b) F. Muller, M. A. Hopkins, N. Coron, M. Gryndberg, L.-C. Brunel, G. Martinez, G. *Rev. Sci. Instrum.* **1989**, *60*, 3681.
[24] Sheldrick, G. M. SHELXTL-Plus, *vers.* 5.1 Structure Determination Software Programs; Bruker-AXS Inc. Madison, WI, **1998**.
[25] Neese, F. *ORCA - an ab initio, Density Functional and Semiempirical Program Package*; University of Bonn, Germany, **2007**.
[26] a) A. D. Becke, *Phys. Rev. A* **1988**, *38*, 3098; b) J. P. Perdew, *Phys. Rev. B* **1986**, *33*, 8822.
[27] A. Schäfer, C. Huber, R. Ahlrichs, *J. Chem. Phys.* **1994**, *100*, 5829.
[28] F. Neese, *J. Chem. Phys.* **2007**, *127*, 164112.
[29] F. Neese, E. I. Solomon, *Inorg. Chem.* **1998**, *37*, 6568.

Received: March 9, 2008
Published online: June 9, 2008

